BIOMAGNETO-HYDRODYNAMIC WILLIAMSON FLUID FLOW AND HEAT TRANSFER OVER A STRETCHING SURFACE: A SPECTRAL QUASI-LINEARIZATION APPROACH

Kairavadi Suresh Babu[b], **Vangala Sugunamma**[a], **Vamsi Krishna Narla**[c]

[a]Sri Venkateswara University, Tirupati, AP, 517502, India
[b]Gokaraju Rangaraju Institute of Engineering and Technology, TG, India
[c]GITAM Deemed to be University, Department of Mathematics, Hyderabad, 502329, India
[*]Corresponding Author e-mail: vnarla@gitam.edu

The flow and heat transfer of a Williamson fluid subjected to a magnetic field are analyzed and investigated through the spectral quasi-linearization method (SQLM). The equations concerned with momentum and energy are obtained from the Navier-Stokes equations, accounting for non-Newtonian effects, viscous dissipation, magnetic forces, and the Lorentz force. The electrically conductive fluid's interaction with the magnetic field produces the Lorentz force, which strongly modifies flow behaviour by exerting a resistive force against the fluid's velocity. The method efficiently linearises the non-linear equations, enabling accurate solutions through the spectral method. Numerical results highlight the influence of Williamson fluid parameters, magnetic field intensity, and heat sources on velocity and temperature fields, offering insights into the fluid's behaviour in industrial applications involving non-Newtonian fluids and magnetic fields.

Keywords: *Williamson fluid; Heat source parameter; Magnetic dipole; Lorentz force and Spectral quasi linearization method*
PACS: 47.50.-d; 47.65.Cb; 65.20.Jk; 03.30.+p; 02.70.Hm; 52.75.Fk, 84.60.Lw.

NOMENCLATURE

S	Cauchy stress tensor	u	velocity component of fluid in x direction
b	Specific body force vector	v	velocity component of fluid in y direction
C_f	Skin friction coefficient	**Greek Symbols**	
H	Magnetic field	α	Magnetic field strength
Ha	Hartmann number	β	Ferromagnetic interaction parameter
K	Pyromagnetic coefficient	ϵ	Dimensionless temperature parameter
k	Thermal conductivity	η	Similarity variable
M	Magnetization	Λ	Thermal relaxiation parameter
Nu	Nusselt number	λ	Dissipation factor,
Pr	Prandtl number	μ	Dynamic viscosity
Q_s	Heat source parameter	μ_0	Magnetic permeability
We	Weissenberg number	ϕ	Magnetic scalar potential
a	Distance of magnetic dipole	ρ	fluid density
C_p	Specific heat	σ	Stefan-Boltzmann constant
T	Temperature	θ	Dimensionless temperature
T_c	Curie temperature	ϑ	Kinematic viscosity
T_w	Temperature at surface		

1. INTRODUCTION

The study of non-Newtonian fluid dynamics over-stretching sheets has become increasingly significant in recent years, owing to its relevance in numerous industrial and engineering applications, such as plastic films, paper, and glass fibres. The continuous deforming boundary condition that a stretching sheet produces influences the fluid's motion and heat transfer properties. Understanding this

phenomenon is essential to optimising cooling and stretching processes in materials. A constitutive model explaining the connection between shear stress and shear rate was put forth by Williamson [1] in 1929, and it has subsequently been used to tackle a number of flow-related issues. The fluid model is better suited to describe complex fluids found in extrusion and spinning processes, as well as polymeric solutions, because it takes into account a decreasing viscosity with increasing shear rate. Numerous investigations have focused on the flow of non-Newtonian fluids across stretching sheets, such as Williamson's fluid [2]-[7]. The analysis of flow and heat transfer of ferrofluids across a stretched sheet under the influence of a dipole magnet has significant technical and industrial applications. The unique properties of ferrofluids in a carrier fluid may be controlled by applying external magnetic fields [8, 9, 10]. E.E. Tzirtzilakis developed a model for analysing mathematically the flow of blood, which is induced by magnetic fields [11]. Magnetic forces are incorporated into the Navier-Stokes equations and solved through numerical methods. Magnetic fields substantially influence blood circulation, potentially facilitating targeted magnetic therapy. Daneshvar Garmroodi et al. [12] conducted numerical simulations of free convection in non-Newtonian ferrofluids in a cavity that is porous and elliptical with a non-uniform magnetic field. The presence of a magnetic field markedly enhanced the transfer of heat, particularly when the wire was positioned at the centre of the elliptical walls. Shear-thinning fluids further augmented the average Nusselt number. AbuHamdeh et al. [13] examined the dynamics of magnetic nanoparticles in the context of a magnetic field within non-Newtonian blood vessels. Their research illustrated the significance of considering non-Newtonian fluid characteristics to enhance drug delivery precision. Srinu and Sreerama [14] investigated the influence of thermal slips and velocity on Williamson's fluid flow across a stretching sheet in the presence of a magnetic field that was inclined and radiation. Abbas et al. [15] investigated flow and heat transmission of magnetohydrodynamic Williamson nanofluid across a stretching sheet (non-linear) that was contained in a porous medium. It was found that with a rise in the Williamson fluid parameter, the concentration profile rises and the velocity declines. It was concluded that rising mass concentration and temperature are caused by increasing Eckert number Ec. As Q, the heat-generating parameter rises, the temperature profile rises, and a reduction in concentration is noticed. The results showed that the profiles of both temperature and concentration trended upward with an increase in the magnetic field parameter M, while the velocity field trended downward. Rashid et al. [16] looked at how a generated magnetic force affected Williamson fluid's flow within a curved channel. It was noticed that compared to a viscous fluid, for a Williamson fluid, the rise in pressure is higher, and the generated magnetic field's magnitude is smaller. Further, the velocity was observed to be small in comparison with a Newtonian fluid. M.V. Krishna and B.V. Swarnalathamma, in their work [17], studied the flow of a MHD Williamson's fluid, which was electrically conducting and heat transfer in the planar symmetrical channel. Obalalu et al. [18] in their work addressed the Hall effect on the flow of Williamson's fluid across a channel that was considered inclined and stretching. In addition, their model took into consideration the impacts of solar radiation, chemical reactions, heat generation or absorption, and activation energy. The graphical results indicated that the heat sink exhibits a thermal efficiency ranging from 4.4% to 5.0%, which was lower compared to that of the heat source. The flow of Williamson fluid diminishes in the magnetic field's presence because of Lorentz force acting opposite to flow direction, which can be considered an application in wired technology. Kashif et al. [19] examined the transport of mass and heat of a MHD Williamson's fluid across a stretched permeable layered plate. The study's findings demonstrate that augmenting the parameter for Brownian motion (Nb) and Thermophoresis (Nt) results in elevated local Nusselt number, signifying enhanced heat transfer rates.

Analyzing the influence of nanofluid properties and magnetic fields can deepen the understanding of heat and mass transport characteristics. Such insights can potentially enhance the performance of ferrofluid-based devices across diverse applications. Recent developments have primarily concentrated on creating efficient numerical techniques for resolving complex, nonlinear differential equations that control fluid flow dynamics [20],[21]. The Spectral Quasi-Linearization Method (SQLM) [22] integrates spectral methods with the quasilinearization technique to achieve high accuracy in linearisation and solving nonlinear terms. Numerous fluid flow applications have benefited from the successful application of this technique, such as the study of boundary layer flows in non-Darcy porous media across sheets that are stretching or shrinking (see, [23]-[27]). Tzirtzilakis and Tanoudis [28] have investigated heat transfer and flow of biomagnetic fluid in magnetic fields using the Chebyshev pseudospectral method (CPSM). CPSM is more accurate and efficient than finite difference methods. The study shows that flow characteristics are significantly influenced by the biomagnetic interaction parameter and that CPSM performs well in this application. Some related literatures are cited in references ([29]-[33]).

The ferrofluid flow and heat transfer of a couple of stress fluids are analysed in the present study. The Spectral Quasi-Linearization Method (SQLM) is utilised to solve flow-governing equations numerically, incorporating the effects of couple stresses and magnetic forces. The equations are converted using similarity variables. We systematically examine effects on the profiles of velocity and temperature of important parameters like the couple stress parameter, ferromagnetic interaction parameter, Prandtl number, heat source parameter, and Hartmann number. The findings show how these parameters impact the flow and thermal properties of ferrofluids and offer comprehensive insights into the intricate interactions between them.

2. FLUID MODEL

A problem of fluid flow across a flat, stretchable sheet stretched in x-direction with velocity $u = cx$ is the primary focus of this analysis, where c is a stretching constant as shown in Fig.(1). At a distance $'a'$ from the centre of sheet, a magnetic dipole is located. In Fig.(1), the symbols S and N denote the South and North Poles of the dipole, respectively. Deformation of fluid in y-direction is a result of the flow being magnetised and saturated. The equations for an incompressible Williamson fluid flow given as:

$$\nabla.V = 0 \tag{1}$$

$$\rho \frac{dV}{dt} = \nabla \mathbf{S} + \rho b \tag{2}$$

The following is an expression of the Williamson fluid model's basic equations:

$$\mathbf{S} = -pI + \tau \tag{3}$$

where

$$\tau = \mu_\infty + \left(\frac{\mu_0 - \mu_\infty}{1 - \Gamma\dot{\gamma}} \right) A \tag{4}$$
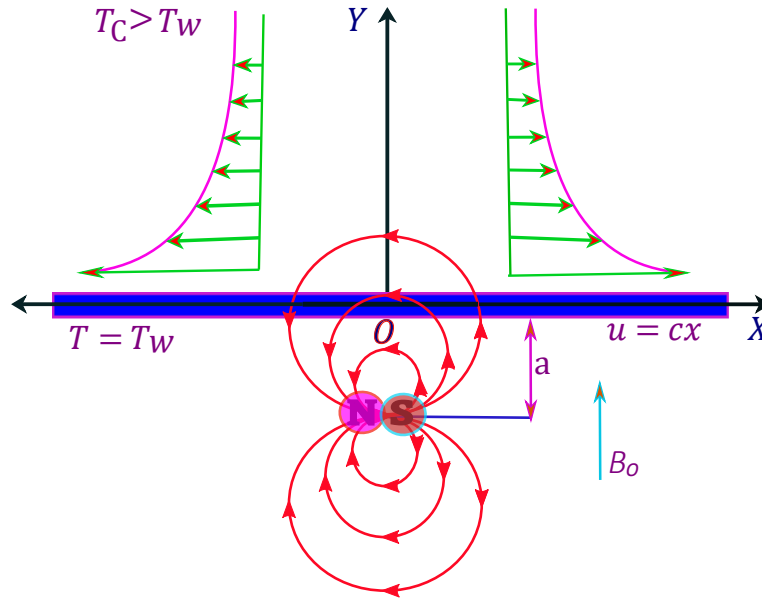
Figure 1. Illustration of physical problem

p stands for pressure, I for identity vector, τ for extra stress tensor, μ_0 and μ_∞ for limiting viscosities at zero and infinite shear rates, respectively, $\Gamma > 0$ for time constant, A for first Rivlin-Erickson tensor. Here $\dot{\gamma}$ is defined as follows:

$$\dot{\gamma} = \sqrt{\frac{1}{2}\pi} \tag{5}$$

$$where \quad \pi = \text{Trace}(A^2), \quad A = \nabla \bar{q} + \nabla \bar{q}^{Tr}$$

$$\nabla \bar{q} = \begin{bmatrix} \frac{\partial u}{\partial x} & \frac{\partial u}{\partial y}, & \frac{\partial v}{\partial x} & \frac{\partial v}{\partial y} \end{bmatrix},$$

by substituting in (5), we get:

$$\dot{\gamma} = \left[2\left[\left(\frac{\partial u}{\partial x}\right)^2 + \left(\frac{\partial v}{\partial y}\right)^2 \right] + \left(\frac{\partial u}{\partial y} + \frac{\partial v}{\partial x}\right)^2 \right]^{\frac{1}{2}} \tag{6}$$

for $\mu_\infty = 0$ and $\Gamma\dot{\gamma} < 1$ and hence, the extra stress tensor takes the form:

$$\tau = \left(\frac{\mu_0}{1 - \Gamma\dot{\gamma}}\right)A \tag{7}$$

by using binomial expansion, we get:

$$\tau = \mu_0\left(1 + \Gamma\dot{\gamma}\right)A \tag{8}$$

When the boundary layer approximations are applied, the continuity, momentum, and energy equations governing the flow take the following form:

$$\frac{\partial u}{\partial x} + \frac{\partial v}{\partial y} = 0 \tag{9}$$

$$\rho\left[u\frac{\partial u}{\partial x} + v\frac{\partial u}{\partial y}\right] = \mu\left(\frac{\partial^2 u}{\partial y^2}\right) + 2\mu\Gamma\frac{\partial u}{\partial y}\frac{\partial^2 u}{\partial y^2} + \mu_0 M\frac{\partial H}{\partial x} - \sigma B_0^2 u \tag{10}$$

$$(\rho C_p)\left[u\frac{\partial T}{\partial x} + v\frac{\partial T}{\partial y}\right] + \mu_0 T\frac{\partial M}{\partial T}\left[u\frac{\partial H}{\partial x} + v\frac{\partial H}{\partial y}\right] + \lambda\left[\left(u\frac{\partial u}{\partial x} + v\frac{\partial u}{\partial y}\right)\frac{\partial T}{\partial x}\right.$$

$$\left. + \left(u\frac{\partial v}{\partial x} + v\frac{\partial v}{\partial y}\right)\frac{\partial T}{\partial y} + u^2\frac{\partial^2 T}{\partial x^2} + v^2\frac{\partial^2 T}{\partial y^2} + 2uv\frac{\partial^2 T}{\partial x\partial y}\right] \tag{11}$$

$$= k\left[\frac{\partial^2 T}{\partial x^2} + \frac{\partial^2 T}{\partial y^2}\right] + Q(T_c - T) + \sigma B_0^2 u$$

The assumed boundary conditions for resolving the aforementioned equations are as follows:

$$u(x,0) = cx, \; v(x,0) = 0, \; T = T_w \; \text{at} \; y = 0,$$
$$u(x,\infty) \to 0, \; T(x,\infty) \to T_c \; \text{at} \; y \to \infty. \tag{12}$$

The potential of magnetic dipole can be found by $\phi(x, y) = \frac{\alpha}{2\pi}\left[\frac{x}{x^2+(y+a)^2}\right]$. We arrive at the conclusion $H = [H_x^2 + H_y^2]^{\frac{1}{2}}$ by employing a linear correlation between magnetic body force and the gradient of H. $M = K(T_c - T)$ is a linear equation that approximates the relationship between magnetization M and temperature T.

The equations considered for transformation are

$$(\xi, \eta) = \frac{(x, y)}{\sqrt{\frac{\nu}{c}}}, \quad u = cxf'(\eta), \quad v = -\sqrt{c\nu}f(\eta) \quad and \quad \theta(\xi, \eta) = \frac{T_c - T}{T_c - T_\omega} = \theta_1(\eta) + \xi^2\theta_2(\eta) \tag{13}$$

u, v the components of velocity satisfy the continuity equation (9). By substituting equations (10) and (11) in (13) and equating the coefficients of ξ^0, ξ and ξ^2, the following equations are obtained:

$$f''' + ff'' - (f')^2 + Wef''f''' - \frac{2\beta\theta_1}{(\eta + \bar{d})^4} - Haf' = 0, \tag{14}$$

$$\theta_1'' + Pr[f\theta_1' - Q_s\theta_1] - \lambda\beta(\epsilon - \theta_1)\left[\frac{2f}{(\eta + \bar{d})^3}\right] - \Lambda\left(ff'\theta_1' + f^2\theta_1''\right) + 2\theta_2 = 0, \tag{15}$$

$$\theta_2'' + Pr[f\theta_2' - 2f'\theta_2 - Q_s\theta_2] + \lambda\beta(\epsilon - \theta_1)\left[\frac{2f'}{(\eta + \bar{d})^4} + \frac{4f}{(\eta + \bar{d})^5}\right] + \frac{2\lambda\beta f\theta_2}{(\eta + \bar{d})^3}$$
$$+ \Lambda\left(-4f'^2\theta_2 + 3ff'\theta_2' - f^2\theta_2'' + 2ff''\theta_2\right) - \lambda Haf'^2 = 0. \tag{16}$$

The following are the transformed boundary conditions:

$$f(0) = 0, \ f'(0) = 1, \ \theta_1(0) = 1, \ \theta_2(0) = 0$$
$$f'(\infty) = 0, \ \theta_1(\infty) = 0, \ \theta_2(\infty) = 0 \tag{17}$$

The remaining non-dimensional variables in the aforementioned converted equations are specified as :

$$\Lambda = \frac{\lambda c\nu}{k}, \quad \beta = \frac{\alpha\mu_0}{2\pi}\frac{\rho K(T_c - T_w)}{\mu^2}, \quad Pr = \frac{(\rho C_p)\vartheta}{k}, \quad We = 2\Gamma x\sqrt{\frac{c^3}{\nu}}$$

$$\lambda = \frac{\mu^2 c}{\rho k(T_c - T_w)}, \quad \epsilon = \frac{T_c}{T_c - T_w}, Ha = \frac{\sigma B_0^2}{\rho c}, \quad Q_s = \frac{Q}{c\rho C_p}.$$

3. SPECTRAL QUASI LINEARIZATION

The spectral quasi-linearization procedure has been applied to obtain the numerical solution of the nonlinear coupled equations (14) to (16), in accordance with the boundary conditions (17). The quasi-linearization technique is applied to equations (14) to (17), yielding the following equations:

$$e_{1,r}f'''_{r+1} + e_{2,r}f''_{r+1} + e_{3,r}f'_{r+1} + e_{4,r}f_{r+1} + e_{5,r}(\theta_1)_{r+1} = S_1, \tag{18}$$

$$e_{6,r}f'_{r+1} + e_{7,r}f_{r+1} + e_{8,r}(\theta_1)''_{r+1} + e_{9,r}(\theta_1)'_{r+1} + e_{10,r}(\theta_1)_{r+1} + e_{11,r}(\theta_2)_{r+1} = S_2, \tag{19}$$

$$e_{12,r}f''_{r+1} + e_{13,r}f'_{r+1} + e_{14,r}f_{r+1} + e_{15,r}(\theta_1)_{r+1} + e_{16,r}(\theta_2)''_{r+1} + e_{17,r}(\theta_2)'_{r+1} + e_{18,r}(\theta_2)_{r+1} = S_3, \tag{20}$$

The boundary conditions are:

$$f_{r+1} = 0, f'_{r+1} = 1, (\theta_1)_{r+1} = 1, (\theta_2)_{r+1} = 0 \ \text{at} \ \eta = 0,$$
$$f'_{r+1} = 0, (\theta_1)_{r+1} = 0, (\theta_2)_{r+1} = 0 \ \text{at} \ \eta \to \infty. \tag{21}$$

The coefficients are obtained as

$$e_{1,r} = Wef''_r + 1, \quad e_{2,r} = f_r + Wef'''_r, \quad e_{3,r} = -2f'_r - Ha, \quad e_{4,r} = f''_r, \quad e_{5,r} = \frac{-2\beta}{(\eta + \bar{d})^4},$$

$$e_{6,r} = -\Lambda f_r(\theta_1')_r, \quad e_{7,r} = Pr(\theta_1')_r - \frac{2\lambda\beta\epsilon}{(\eta + \bar{d})^3} + \frac{2\lambda\beta(\theta_1)_r}{(\eta + \bar{d})^3} - \Lambda f_r'(\theta_1')_r - 2\Lambda f_r(\theta_1'')_r,$$

$$e_{8,r} = 1 - \Lambda f_r^2, \quad e_{9,r} = Prf_r - \Lambda f_r f_r', \quad e_{10,r} = \frac{2\lambda\beta f_r}{(\eta + \bar{d})^3} - PrQ_s, e_{11,r} = 2,$$

$$e_{12,r} = 2\Lambda f_r(\theta_2)_r, \quad e_{13,r} = -2Pr(\theta_2)_r + \frac{2\lambda\beta\epsilon}{(\eta + \bar{d})^4} - \frac{2\lambda\beta(\theta_1)_r}{(\eta + \bar{d})^4} - 8\Lambda f_r'\theta_2 + 3\Lambda f_r(\theta_2')_r - 2\lambda Haf',$$

$$e_{14,r} = Pr(\theta_2')_r + \frac{2\lambda\beta(\theta_2)_r}{(\eta + \bar{d})^3} + \frac{4\lambda\beta\epsilon}{(\eta + \bar{d})^5} - \frac{4\lambda\beta(\theta_1)_r}{(\eta + \bar{d})^5} + 3\Lambda f_r'(\theta_2')_r - 2\Lambda f_r(\theta_2'')_r + 2\Lambda f_r''(\theta_2)_r,$$

$$e_{15,r} = \frac{-2\lambda\beta f_r'}{(\eta + \bar{d})^4} - \frac{4\lambda\beta f_r}{(\eta + \bar{d})^5}, \quad e_{16,r} = 1 - \Lambda f_r^2, \quad e_{17,r} = Prf_r + 3\Lambda f_r'f_r,$$

$$e_{18,r} = -2Prf_r' - PrQ_s + \frac{2\lambda\beta f_r}{(\eta + \bar{d})^3} - 4\Lambda(f_r')^2 + 2\Lambda f_r f_r'',$$

$$S_1 = f_r f_r'' - f_r'^2 + We f_r'' f_r''', \quad S_2 = -\Lambda f_r' f_r \theta_r' - \Lambda (f_r)^2 (\theta_1'')_r + Pr f_r (\theta_1')_r + \frac{2\lambda\beta f_r (\theta_1)_r}{(\eta + \bar{d})^3},$$

$$S_3 = -\lambda Ha((f')^2)_r - 2Pr f_r' (\theta_2)_r + Pr f_r (\theta_2')_r + \frac{2\lambda\beta f_r (\theta_2)_r}{(\eta + \bar{d})^3} - \frac{2\lambda\beta f_r' (\theta_1)_r}{(\eta + \bar{d})^4} - \frac{4\lambda\beta (\theta_1)_r f_r}{(\eta + \bar{d})^5} - 3\Lambda f_r' f_r (\theta_2')_r$$

$$- \Lambda (f^2)_r (\theta_2'')_r + 2\Lambda f_r'' f_r (\theta_2)_r - (4(f')^2)_r (\theta_2)_r.$$

Equations (14)–(17) are solved numerically using the pseudo-spectral Chebyshev collocation method. In this framework, initially, the semi-infinite range $\eta \in [0, \infty)$ is truncated to $\eta \in [0, L_\infty]$, where $L_\infty \in \mathbb{Z}^+$. This range $[0, L_\infty]$ is transformed into $[-1, 1]$ using the transformation variable $\eta = L_\infty(1 + \zeta)/2$. Using the differential matrix $\mathbf{D}$ for Chebyshev polynomials (see, [27]), the derivatives of the unknown functions $f(\eta)$, $\theta_1(\eta)$, and $\theta_2(\eta)$ are derived at the collocation points of the product matrix vector as follows:

$$\frac{\partial^p f_{r+1}}{\partial \eta^p} = \left(\frac{2}{L}\right)^p \sum_{i=0}^{N} D_{N,i}^p f_{r+1}(\eta_i) = \mathbf{D}^p F,$$

$$\frac{\partial^p (\theta_1)_{r+1}}{\partial \eta^p} = \left(\frac{2}{L}\right)^p \sum_{i=0}^{N} D_{N,i}^p (\theta_1)_{r+1}(\eta_i) = \mathbf{D}^p \Theta_1, \tag{22}$$

$$\frac{\partial^p (\theta_2)_{r+1}}{\partial \eta^p} = \left(\frac{2}{L}\right)^p \sum_{i=0}^{N} D_{N,i}^p (\theta_2)_{r+1}(\eta_i) = \mathbf{D}^p \Theta_2.$$

The Chebyshev differentiation matrix $\mathbf{D}$ is scaled by $L_\infty/2$. The matrix $\mathbf{D}$ in this instance has a derivative order of p and an order of $(N + 1) \times (N + 1)$. Using $\zeta_j = \cos(\pi j/N)$, $j = 1, 2, \cdots N$, where N denotes number of collocation points, the Gauss-Lobatto points are constructed to characterize nodes in $[-1, 1]$. Substituting Eq. (22) into Eqs. (18)-(21), we obtain

$$[e_{1,r}\mathbf{D}^3 + e_{2,r}\mathbf{D}^2 + e_{3,r}\mathbf{D} + e_{4,r}I] f_{r+1} + e_{5,r}(\theta_1)_{r+1} = S_1, \tag{23}$$

$$[e_{6,r}\mathbf{D} + e_{7,r}I] f_{r+1} + [e_{8,r}\mathbf{D}^2 + e_{9,r}\mathbf{D} + e_{10,r}I](\theta_1)_{r+1} + [e_{11,r}I](\theta_2)_{r+1} = S_2, \tag{24}$$

$$[e_{12,r}\mathbf{D}^2 + e_{13,r}\mathbf{D} + e_{14,r}I] f_{r+1} + e_{15,r}(\theta_1)_{r+1} + [e_{16,r}\mathbf{D}^2 + e_{17,r}\mathbf{D} + e_{18,r}I](\theta_2)_{r+1} = S_3. \tag{25}$$

Applying spectral method on the boundary conditions gives

$$\sum_{k=0}^{N} \mathbf{D}_{N,k} f_{r+1}(\zeta_0) = 0, \ (\theta_1)_{r+1}(\zeta_0) = 0, \ (\theta_2)_{r+1}(\zeta_0) = 0, \ f_{r+1}(\zeta_N) = 0,$$

$$\sum_{k=0}^{N} \mathbf{D}_{N,k} f_{r+1}(\zeta_N) = 1, \ (\theta_1)_{r+1}(\zeta_N) = 1, \ (\theta_2)_{r+1}(\zeta_N) = 0.$$

The above system of equations expressed in matrix form as:

$$\begin{bmatrix} \mathbf{K}_{11} & \mathbf{K}_{12} & \mathbf{K}_{13} \\ \mathbf{K}_{21} & \mathbf{K}_{22} & \mathbf{K}_{23} \\ \mathbf{K}_{31} & \mathbf{K}_{32} & \mathbf{K}_{33} \end{bmatrix} \times \begin{bmatrix} F_{r+1} \\ \Theta_{1r+1} \\ \Theta_{2r+1} \end{bmatrix} = \begin{bmatrix} S_1 \\ S_2 \\ S_3 \end{bmatrix}, \tag{26}$$

The boundary conditions are placed on the separate matrices as follows:

$$\mathbf{K}_{11} = \begin{bmatrix} \mathbf{D}_{0,0} & \mathbf{D}_{0,1} & \cdots & \mathbf{D}_{0,N-1} & \mathbf{D}_{0,N} \\ & & K_{11} & & \\ \mathbf{D_{N-1,0}} & \mathbf{D_{N-1,1}} & \cdots & \mathbf{D_{N-1,N-1}} & \mathbf{D_{N-1,N}} \\ 0 & 0 & \cdots & 0 & 1 \end{bmatrix}, \quad \mathbf{K}_{12} = \begin{bmatrix} 0 & 0 & \cdots & 0 & 0 \\ & & K_{12} & & \\ 0 & 0 & \cdots & 0 & 0 \\ 0 & 0 & \cdots & 0 & 0 \end{bmatrix},$$

$$\mathbf{K}_{13} = \begin{bmatrix} 0 & 0 & \cdots & 0 & 0 \\ & & K_{13} & & \\ 0 & 0 & \cdots & 0 & 0 \\ 0 & 0 & \cdots & 0 & 0 \end{bmatrix}, \mathbf{K}_{21} = \begin{bmatrix} 0 & 0 & \cdots & 0 & 0 \\ & & K_{21} & & \\ 0 & 0 & \cdots & 0 & 0 \end{bmatrix}, \quad \mathbf{K}_{22} = \begin{bmatrix} 1 & 0 & \cdots & 0 & 0 \\ & & K_{22} & & \\ 0 & 0 & \cdots & 0 & 1 \end{bmatrix},$$

$$\mathbf{K}_{23} = \begin{bmatrix} 0 & 0 & \cdots & 0 & 0 \\ & & K_{23} & & \\ 0 & 0 & \cdots & 0 & 0 \end{bmatrix}, \quad \mathbf{K}_{31} = \begin{bmatrix} 0 & 0 & \cdots & 0 & 0 \\ & & K_{31} & & \\ 0 & 0 & \cdots & 0 & 0 \end{bmatrix}, \quad \mathbf{K}_{32} = \begin{bmatrix} 0 & 0 & \cdots & 0 & 0 \\ & & K_{32} & & \\ 0 & 0 & \cdots & 0 & 0 \end{bmatrix},$$

$$\mathbf{K}_{33} = \begin{bmatrix} 1 & 0 & \cdots & 0 & 0 \\ & & K_{33} & & \\ 0 & 0 & \cdots & 0 & 1 \end{bmatrix}, \quad \mathbf{F}_{r+1} = \begin{bmatrix} f_{r+1,0} \\ \vdots \\ f_{r+1,N-1} \\ f_{r+1,N} \end{bmatrix}, \quad \mathbf{\Theta}_{1r+1} = \begin{bmatrix} \theta_{1r+1,0} \\ \vdots \\ \vdots \\ \theta_{1r+1,N} \end{bmatrix},$$

$$\mathbf{\Theta_{2r+1}} = \begin{bmatrix} \theta_{2r+1,0} \\ \vdots \\ \vdots \\ \theta_{2r+1,N} \end{bmatrix}, \quad S_1 = \begin{bmatrix} 0 \\ \mathbf{s_1} \\ 1 \\ 0 \end{bmatrix}, \quad S_2 = \begin{bmatrix} 0 \\ \mathbf{s_2} \\ 1 \end{bmatrix}, \quad S_3 = \begin{bmatrix} 0 \\ \mathbf{s_3} \\ 0 \end{bmatrix},$$

where

$$K_{11} = [\text{diag}(e_{1,r}) \quad \text{diag}(e_{2,r}) \quad \text{diag}(e_{3,r}) \quad \text{diag}(e_{4,r})][\mathbf{D}^3 \quad \mathbf{D}^2 \quad \mathbf{D} \quad I]^T,$$

$$K_{12} = \text{diag}(e_{5,r}), \quad K_{13} = 0,$$

$$K_{21} = [\text{diag}(e_{6,r}) \quad \text{diag}(e_{7,r})][\mathbf{D} \quad I]^T,$$

$$K_{22} = [\text{diag}(e_8, r) \quad \text{diag}(e_{9,r}) \quad \text{diag}(e_{10,r})][\mathbf{D}^3 \quad \mathbf{D}^2 \quad \mathbf{D} \quad I]^T, \quad K_{23} = [\text{diag}(e_{11,r})]I,$$

$$K_{31} = [\text{diag}(e_{12,r}) \quad \text{diag}(e_{13,r}) \quad \text{diag}(e_{14,r})][\mathbf{D}^2 \quad \mathbf{D} \quad I]^T, \quad K_{32} = \text{diag}(e_{15,r}),$$

$$K_{33} = [\text{diag}(e_{16r}) \quad \text{diag}(e_{17,r}) \quad \text{diag}(e_{18,r})][\mathbf{D}^2 \quad \mathbf{D} \quad I]^T,$$

where e is (N + 1)×(N + 1) diagonal matrix, I, 0 are (N + 1)×(N + 1) unit matrix and zero matrix, respectively.

4. CONVERGENCE ANALYSIS AND RESULTS

The convergence analysis shows that iterative approach convergence to exact solution of the equations (14) and (15), while considering the boundery conditions (17). The residual error quantifies the proximity of the numerical solution to exact solution. The residual error of equations (14) and (15) is represented below:

$$Res(f) = f''' + ff'' - (f')^2 + We f'' f''' - \frac{2\beta\theta_1}{(\eta + \bar{d})^4} - Haf', \tag{27}$$

$$Res(\theta_1) = \theta_1'' + Pr[f\theta_1' - Q_s\theta_1] - \lambda\beta(\epsilon - \theta_1)\left[\frac{2f}{(\eta + \bar{d})^3}\right] - \Lambda\left(ff'\theta_1' + f^2\theta_1''\right) + 2\theta_2. \tag{28}$$

$\|Res(f)\|_\infty$ and $\|Res(\theta_1)\|_\infty$ measure the largest absolute value of the error throughout the domain.
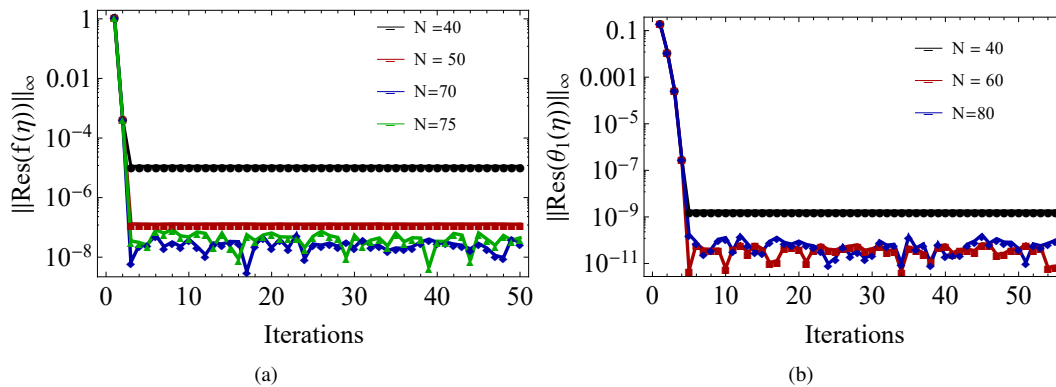

Figure 2. Influence of iterations on $\|Res(f)\|_\infty$ and $\|Res(\theta_1)\|_\infty$ when $Pr = 1$, $\lambda = 0.01$, $Q_s = 0.5$, $\epsilon = 2$, $\beta = 1$, $\Lambda = 0.5$, $Ha = 1$ and $We = 0.01$.

The residual error in f over 50 iterations for several numbers of collocation points (N = 65, 70, 75) is displayed in Fig. (2)(a). The figure shows that the best accuracy is achieved in between the collocation points 65 and 75, with residual errors around 10^{-8}. Similarly, The optimal residuals are achieved around 10^{-11} for the residual errors in θ_1 that is shown in Fig. (2)(b). The accuracy gradually reduces beyond this range of collocation points. From the above results, the numerical approach achieved the best accuracy between 65 to 75 collocation points and performance after the seventh iteration in f and the tenth iteration in θ_1.

The resistance that the fluid applies to the surface as a result of shear stresses is measured by C_f, the skin friction coefficient defined as:

$$C_f = \frac{\tau_w}{\rho U_s^2}$$

where τ_w is the wall shear stress at surface ($y = 0$):

$$\tau_w = \mu\left(1 - \frac{1}{\Gamma\dot{\gamma} + 1}\right)\left(\frac{\partial u}{\partial y}\right)_{y=0}$$

A simplified expression for skin friction coefficient is given as:

$$C_f Re_x^{\frac{1}{2}} = f''(0) + \frac{We}{2} f''(0)^2$$

Table 1. Numerical values of $C_f Re_x^{\frac{1}{2}}$

We	$C_f Re_x^{\frac{1}{2}}$					
	$\beta=0$	$\beta=0.1$	$\beta=0.2$	$\beta=0.3$	$\beta=0.4$	$\beta = 1$
0	-1.095599662	-1.128912975	-1.162233927	-1.195730434	-1.229308197	-1.432427836
0.001	-1.095382958	-1.128657128	-1.162015567	-1.195459333	-1.228989428	-1.43204273
0.1	-1.073084327	-1.105917857	-1.13882558	-1.171808576	-1.204867949	-1.404893248
0.2	-1.048548562	-1.08079605	-1.113097732	-1.145454265	-1.177866314	-1.373542304
0.3	-1.0213007	-1.052721717	-1.084153148	-1.11559285	-1.147038361	-1.335636773
0.4	-0.990052177	-1.02015071	-1.050134304	-1.079979608	-1.109655784	-1.146034455

The Nusselt number for a Williamson fluid over a stretched sheet quantifies the convective heat transfer at the surface in relation to the conductive heat transfer inside the fluid. The following is the definition of the local Nusselt number Nu_x at a distance x from the leading edge:

$$Nu_x = \frac{q_w x}{k(T_w - T_c)}$$

where $q_w = -k\left(\frac{\partial T}{\partial y}\right)_{y=0}$ is the wall heat flux.

The local Nusselt number becomes:

$$Nu_x = -\theta'(0)\sqrt{Re_x}$$

Table 2. Numerical values of $Nu_x Re_x^{\frac{-1}{2}}$

We	$Nu_x Re_x^{\frac{-1}{2}}$					
	$\beta=0$	$\beta=0.1$	$\beta=0.2$	$\beta=0.3$	$\beta=0.4$	$\beta=1$
0	1.073455819	1.068598579	1.068738038	1.064270995	1.060645959	1.042842363
0.001	1.074442179	1.071432388	1.068411953	1.065378014	1.062332056	1.043801078
0.1	1.067971776	1.064767511	1.06154568	1.058306182	1.055048916	1.03512635
0.2	1.06075601	1.057305343	1.053827978	1.050323504	1.046791495	1.024995014
0.3	1.052633942	1.048854466	1.045030664	1.041160916	1.037243449	1.012610756
0.4	1.04319135	1.038916915	1.034552705	1.030089571	1.025515841	0.993059527

Tables (1) and (2) display variations in coefficient of Skin friction and heat transfer rate for different values of Γ and β. Other parameters are maintained at following values: $d = 1$, $\lambda = 0.01$, $\epsilon = 2$, $Pr = 1$, $\Lambda = 0.5$, $Ha = 0.2$, $Qs = 0.5$. From Table (1) it can be noticed that for a fixed β, the drag coefficient increases with a rise in We. The augmentation of the drag coefficient with a rise in Weissenberg number is attributable to the fluid's shear-thinning characteristics, and increased energy dissipation within the flow. Further, it decreases with a rise in β. This is attributed to the stabilising influence of magnetic field, a decrease in flow instabilities, laminar flow development, or alterations in the velocity gradient and shear stress adjacent to the wall. Table (2) depicts a decrease in heat transfer coefficient with a rise in We and β. Higher values of β intensify the effects of magnet in fluid and speed up heat transfer as a consequence of the interaction between ferromagnetic particles in fluid and magnetic field. Better thermal conductivity and more effective heat transfer are encouraged by this interaction. The effects of β, Pr We, Qs, Γ on profiles of velocity and temperature are depicted in (3)-(10). From Figure (3)(a), one can notice that velocity drops from the highest value near the wall where $\eta=0$, towards the free stream value (where $\eta \rightarrow \infty$) with the increment of β. This signifies that enhanced magnetic effects lead to a more rapid deceleration of fluid in boundary layer as β levels rise. Figure 3(b) illustrates that as β is increased, it leads to a more pronounced temperature differential near the wall, indicating a reduced thickness of the thermal boundary layer. Increased values of β facilitate the transfer of heat to fluid from the surface.

Figure 4(*a*) clearly illustrates that the velocity diminishes from its maximum near the wall to the free stream value across different Prandtl numbers Pr. Fluctuations in the Prandtl number exert negligible influence on the thickness of velocity boundary layer, as they do not significantly alter the velocity profile. Figure 4(*b*) illustrates a reduction in temperature profile as Prandtl number (Pr) increases. This suggests that a higher Pr value results in diminished thermal diffusivity, thereby decreasing the efficiency of heat conduction away from the wall. Consequently, there is an elevated rate of temperature change and a reduced temperature near the surface. Fig. (5)(a) and Fig. (5)(b) illustrate the impact of heat source Q_s on profiles of velocity and temperature. Figure 5(*a*) demonstrates a more significant velocity gradient near the wall, signifying a reduction in boundary layer thickness as values of Q_s increase. Figure 5(*b*) shows that elevated values of (Q_s) result in a diminished temperature profile near the wall. The observed phenomena can be attributed to the
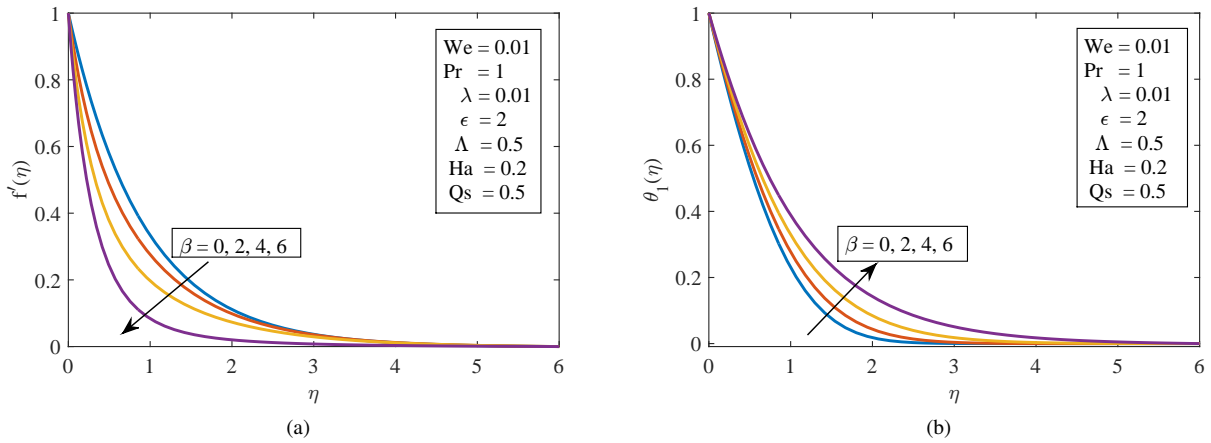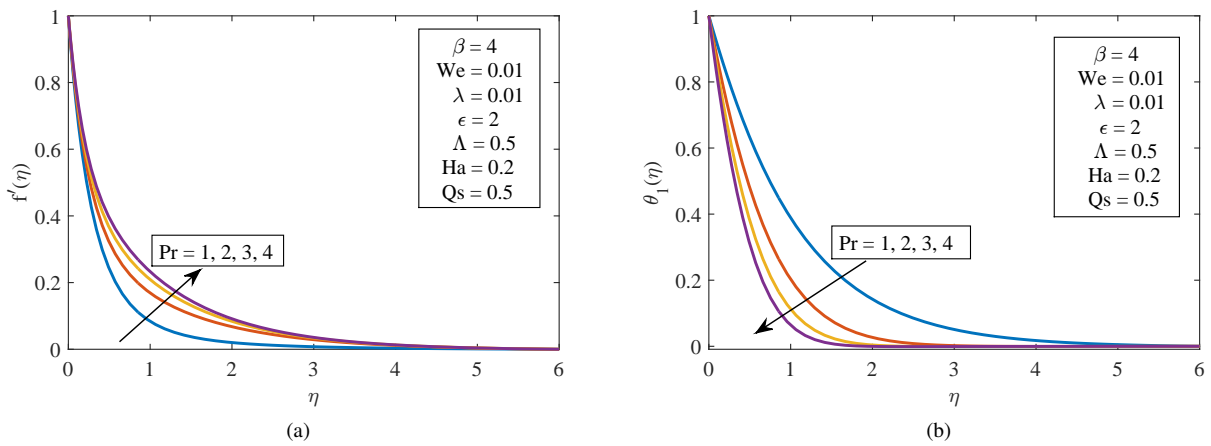
Figure 3. Impact of β on velocity and temperature.

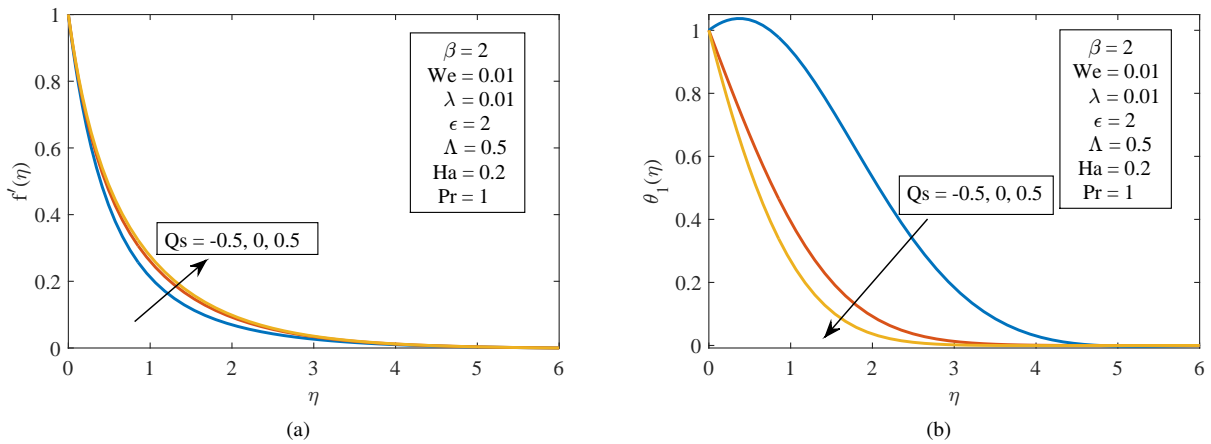**Figure 4.** Impact of Pr on velocity and temperature.

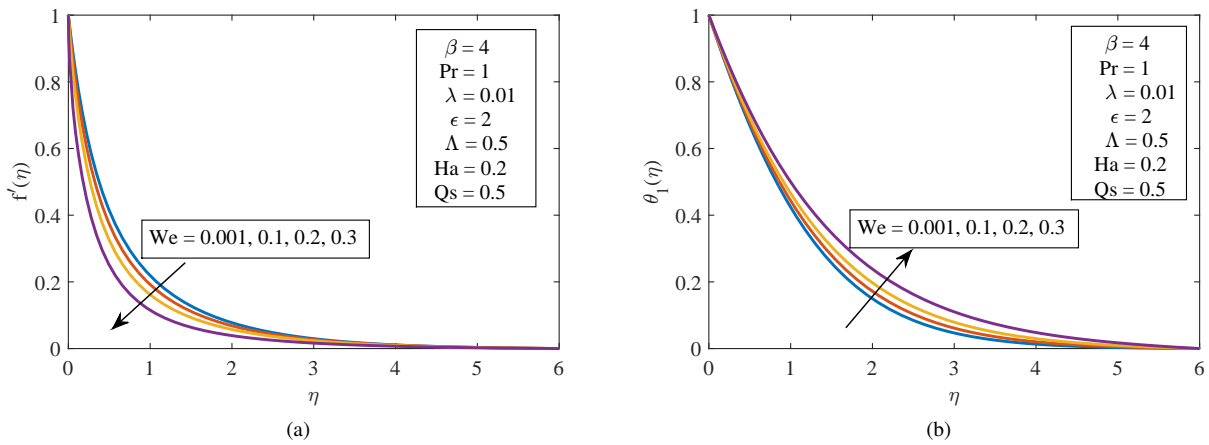**Figure 5.** Impact of Qs on velocity and temperature.
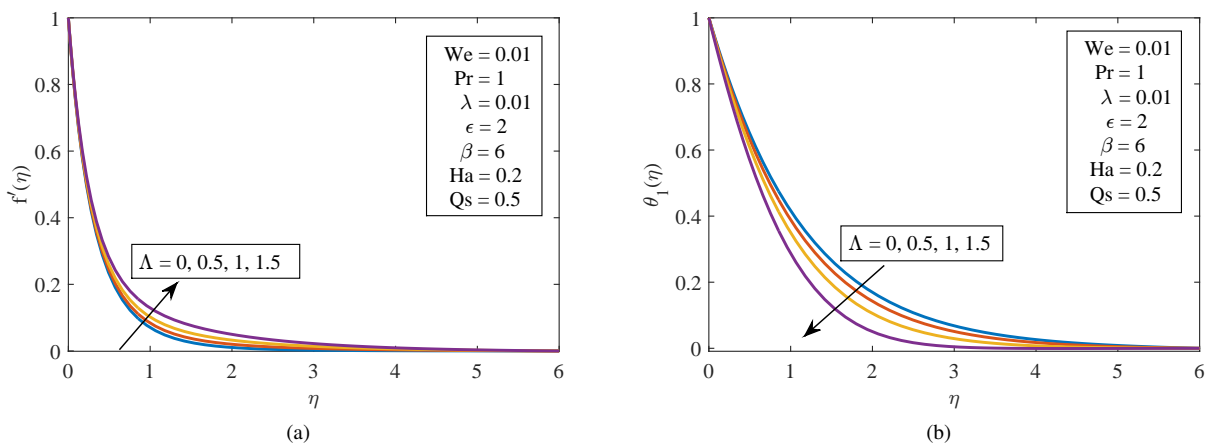
Figure 6. Impact of *We* on velocity and temperature.

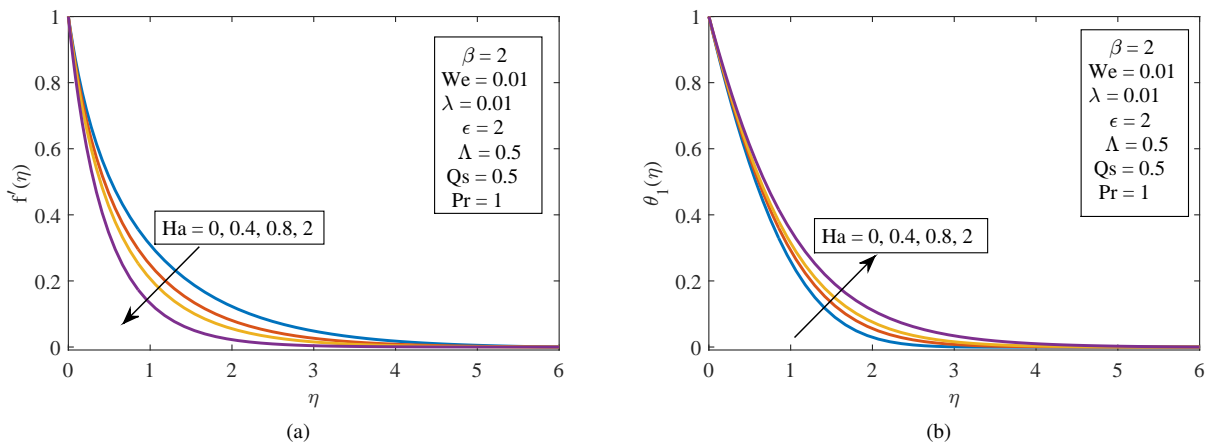**Figure 7.** Impact of Λ on velocity and temperature.

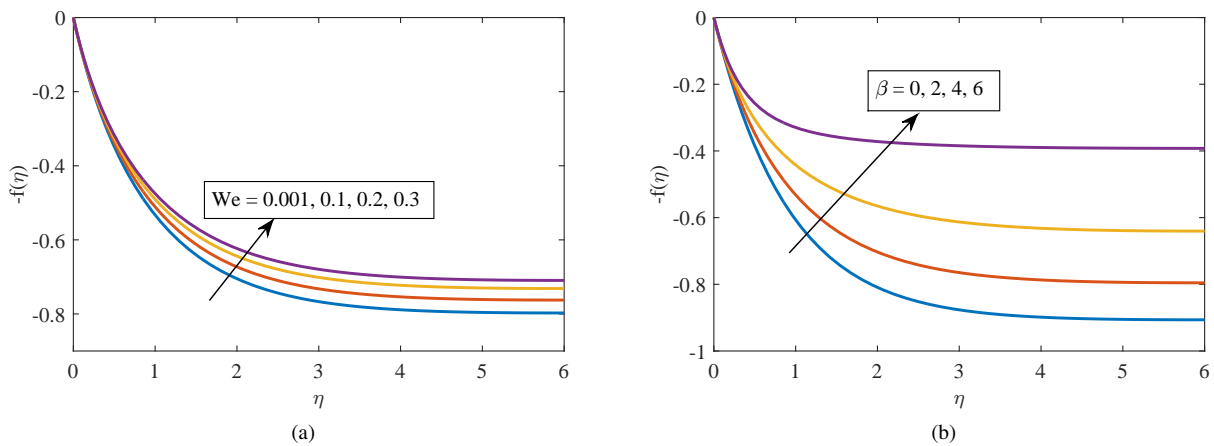**Figure 8.** Impact of *Ha* on velocity and temperature.

Figure 9. Impact of We and β on transverse velocity $-f(\eta)$.
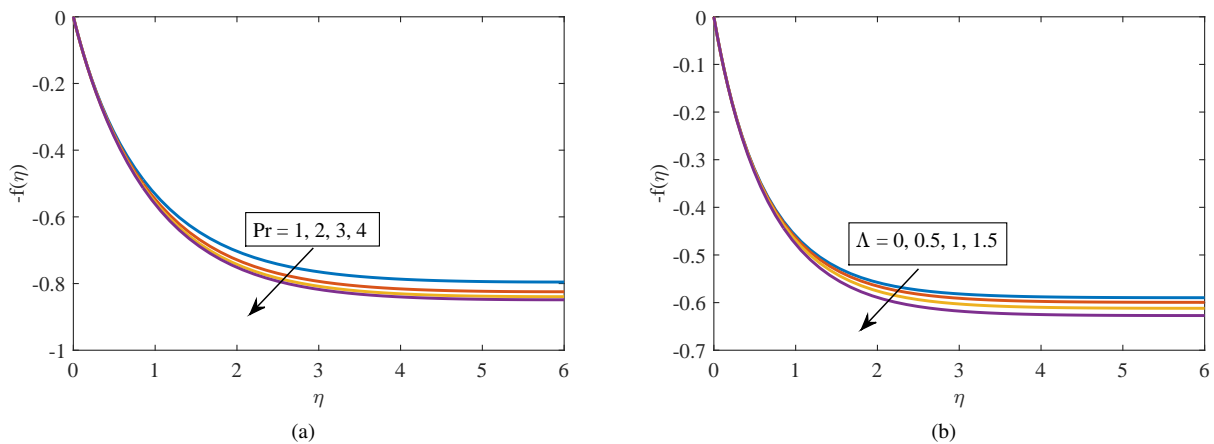

Figure 10. Impact of Pr and Λ on transverse velocity $-f(\eta)$.

increased heat generation in the fluid, which leads to a more uniform distribution of temperature within boundary layer and diminishing temperature variation near the wall.

Fig. (6)(a)-6(b) are depicted to notice the influence of We on profiles of velocity and temperature. Due to the fluid particle's increased relaxation time, the velocity profile decreases as We rises. The thickness of thermal boundary layer decreases as We increases which results in an enhancement in the temperature profile.

Fig. (7)(a) and (7)(b) illustrates a rise in velocity and reduction of temperature as Λ increases. The axial velocity is noticed to increase with a rise Λ due to reduced thermal effects which causes the momentum to increase. With an increase of Λ, a time lag is introduced in the process of heat conduction, which slows the heat diffusion rate due which the reduction in temperature.

Fig. (8)(a) and (8)(b) depict the influence of Ha on profiles of velocity and temperature. A rise in Hartmann number increases the resistive force, leading to reduced flow. The temperature is noticed to increase with a rise in Ha, due to increased viscous dissipation and slowed convective heat transfer. The graphs in figure (9) and (10) are plotted for the values: $\lambda = 0.01$, $\epsilon = 2$, $Pr = 1$, $Ha = 0.2$, $\beta=2$, $Qs = 0.5$, $We=0.01$ and $\Lambda= 0.5$.

Fig. (9) (a) and (9)(b) illustrate the impact of We and β on the transverse velocity. With a rise in both We and β, the elastic and magnetic interactions of fluid are enhanced, leading to an increase in transverse velocity. Figures in (10) illustrate the influence of Pr and Λ on transverse velocity.

The decline in transverse velocity with an elevation of Pr and Λ results from the synergistic effects of heightened viscous dissipation, diminished temperature gradients, and alterations in the fluid's responsiveness to thermal fluctuations.

5. CONCLUSIONS

This article examines the flow and heat transfer characteristics of Williamson fluid over a stretched sheet when a magnetic dipole is present. Equations governing fluid flow are transformed to non-linear ordinary differential equations using similarity transformations. These equations are solved numerically through the Spectral Quasi-Linearization Method. A MATLAB program is utilized to generate

graphical results, facilitating a detailed analysis of the influence of various parameters on the velocity and temperature profiles. The conclusions that can be drawn are:

- An increase of β, We and Ha results in a decline of axial velocity and a rise in temperature, and transverse velocity.

- With higher values of the Qs, Prandtl number Pr, and Thermal relaxation parameter Λ, the temperature declines and velocity rises.

- With an increase in We, coefficient of skin friction reduces and rate of heat transfer rises, while both decrease with a rise in β.

Residual errors for velocity and temperature profiles clearly showed rapid convergence, with a significant improvement in accuracy after the fifth iteration. The optimal accuracy required 40-80 collocation points, after which the accuracy gradually decreased. The residual error norms for different parameters ranged from 10^{-5} to 10^{-11}, indicating the numerical scheme's robustness and efficiency.

The results can be applied to simulate blood flow in the presence of a magnetic field, as blood exhibits non-Newtonian behavior similar to Williamson fluids under certain conditions. This is crucial for designing medical devices like magnetic resonance imaging (MRI) systems or improving techniques for controlling blood flow during surgeries.

In industries dealing with non-Newtonian fluids, the results are vital for optimizing processes such as extrusion and stretching of polymer sheets or films. Understanding heat transfer and fluid flow characteristics ensures better quality control and energy efficiency during production.

ORCID

●**Kairavadi Suresh Babu**, https://orcid.org/0000-0003-1538-1072; ●**Vangala Sugunamma**, https://orcid.org/0000-0001-6815-1540;
●**Vamsi Krishna Narla**, https://orcid.org/0000-0003-0994-3497

REFERENCES

[1] R.V. Williamson, "The Flow of Pseudoplastic Materials," Industrial and Engineering Chemistry, **21**(11), 1108–1111 (1929). https://doi.org/10.1021/ie50239a035

[2] S. Nadeem, S.T. Hussain, and C. Lee, "Flow of a Williamson fluid over a stretching sheet," Brazilian Journal of Chemical Engineering, **30**(3), 619–625 (2013). https://doi.org/10.1590/S0104-66322013000300019

[3] M.Y. Malik, M. Bibi, F. Khan, and T. Salahuddin, "Numerical solution of Williamson fluid flow past a stretching cylinder and heat transfer with variable thermal conductivity and heat generation/absorption," AIP Advances, **6**(3), o35101 (2016). https://doi.org/10.1063/1.4943398

[4] M.I. Khan, S. Qayyum, T. Hayat, M.I. Khan, and A. Alsaedi, "Entropy optimization in flow of Williamson nanofluid in the presence of chemical reaction and Joule heating," International Journal of Heat and Mass Transfer, **133**, 959–967 (2019). https://doi.org/10.1016/j.ijheatmasstransfer.2018.12.168

[5] I. Zehra, M.M. Yousaf, and S. Nadeem, "Numerical solutions of Williamson fluid with pressure dependent viscosity," Results in Physics, **5**, 20–25 (2015). https://doi.org/10.1016/j.rinp.2014.12.002

[6] K. Subbarayudu, S. Suneetha, and P.B.A. Reddy, "The assessment of time dependent flow of Williamson fluid with radiative blood flow against a wedge," Propulsion and Power Research, **9**(1), 87–99 (2019). https://doi.org/10.1016/j.jppr.2019.07.001

[7] A.M. Megahed, "Williamson fluid flow due to a nonlinearly stretching sheet with viscous dissipation and thermal radiation," Journal of the Egyptian Mathematical Society, **27**(1), 12 (2019). https://doi.org/10.1186/s42787-019-0016-y

[8] R.E. Rosensweig, *Ferrohydrodynamics*, (Cambridge University Press, New York, USA, 1985).

[9] H.I. Andersson, and O.A. Valnes, "Flow of a heated ferrofluid over a stretching sheet in the presence of a magnetic dipole," Acta Mechanica, **128**, 39–47, (1998). https://doi.org/10.1007/BF01463158

[10] B.A. Pasha, G. Sowmya, V. Ramachandramurthy, and H.M. Nagesh, "Influence of Heat Source on Thin Film Flow of Ferrofluid Past an Unsteady Stretching Sheet," Journal of Mines Metals and Fuels, **71**(10), 1518–1525 (2023). https://doi.org/10.18311/jmmf/2023/35812

[11] E.E. Tzirtzilakis, "A mathematical model for blood flow in magnetic field," Physics of Fluids, **17**(7), 077103 (2005). https://doi.org/10.1063/1.1978807

[12] M.R.D. Garmroodi, A. Ahmadpour, M.R. Hajmohammadi, and S. Gholamrezaie, "Natural convection of a non-Newtonian ferrofluid in a porous elliptical enclosure in the presence of a non-uniform magnetic field," Journal of Thermal Analysis and Calorimetry, **141**(5), 2127–2143 (2019). https://doi.org/10.1007/s10973-019-09045-3

[13] N.H. Abu-Hamdeh, R.A.R. Bantan, F. Aalizadeh, and A. Alimoradi, "Controlled drug delivery using the magnetic nanoparticles in non-Newtonian blood vessels," Alexandria Engineering Journal, **59**(6), 4049–4062 (2020). https://doi.org/10.1016/j.aej.2020.07.010

[14] N.S. Anagandula, and N.K.S. Reddy, "Velocity and Thermal Slips Impact on the Williamson Fluid Flow above a Stretching Sheet in the Existence of Radiation and Inclined Magnetic Field," CFD Letters, **16**(7), 118–135 (2024). https://doi.org/10.37934/cfdl.16.7.118135

[15] A. Abbas, M.B. Jeelani, A.S. Alnahdi, and A. Ilyas, "MHD Williamson Nanofluid Fluid Flow and Heat Transfer Past a Non-Linear Stretching Sheet Implanted in a Porous Medium: Effects of Heat Generation and Viscous Dissipation," Processes, **10**(6), 1221 (2022). https://doi.org/10.3390/pr10061221

[16] M. Rashid, K. Ansar, and S. Nadeem, "Effects of induced magnetic field for peristaltic flow of Williamson fluid in a curved channel," Physica a Statistical Mechanics and Its Applications, **553**, 123979 (2020). https://doi.org/10.1016/j.physa.2019.123979

[17] M.V. Krishna, and B.V. Swarnalathamma, "Convective heat and mass transfer on MHD peristaltic flow of Williamson fluid with the effect of inclined magnetic field," AIP Conference Proceedings, **1728**, 020461 (2016). https://doi.org/10.1063/1.4946512

[18] A.M. Obalalu, S.O. Salawu, O.A. Olayemi, O.A. Ajala, and K. Issa, "Analysis of hydromagnetic Williamson fluid flow over an inclined stretching sheet with Hall current using Galerkin Weighted Residual Method," Computers & Mathematics With Applications, **146**, 22–32 (2023). https://doi.org/10.1016/j.camwa.2023.06.021

[19] Y.-X. Li, M.H. Alshbool, Y.-P. Lv, I. Khan, M.R. Khan, and A. Issakhov, "Heat and mass transfer in MHD Williamson nanofluid flow over an exponentially porous stretching surface," Case Studies in Thermal Engineering, **26**, 100975 (2021). https://doi.org/10.1016/j.csite.2021.100975

[20] M. Dhivua, and K. Vajravelu, "Heat transfer characteristics of a Williamson fluid flow through a variable porosity regime," International Journal of Ambient Energy, **44**(1), 2553–2568 (2023). https://doi.org/10.1080/01430750.2023.2258378

[21] M.S. Anwar, M.S. Alqarni, and M. Irfan, "Exploring the marvels of heat transfer: "MHD convection at a stagnation point in non-Newtonian fluid with yield stress and chemical reactions," Chinese Journal of Physics, **89**, 1299-1308 (2024). https://doi.org/10.1016/j.cjph.2024.01.030

[22] L.N. Trefethen, *Spectral Methods in MATLAB*, (Oxford University Mathematical Institute, Oxford, United Kingdom, 2000).

[23] D. Srinivasacharya, and K.H. Bindu, "Entropy generation in a micropolar fluid flow through an inclined channel with slip and convective boundary conditions," Energy, **91**, 72–83 (2015). https://doi.org/10.1016/j.energy.2015.08.014

[24] R.A. Alharbey, H. Mondal, and R. Behl, "Spectral Quasi-Linearization Method for Non-Darcy Porous Medium with Convective Boundary Condition," Entropy, **21**(9), 838 (2019). https://doi.org/10.3390/e21090838

[25] H. Mondal, and S. Bharti, "Spectral Quasi-linearization for MHD Nanofluid Stagnation Boundary Layer Flow due to a Stretching/Shrinking Surface," Journal of Applied and Computational Mechanics, **6**(4), 1058–1068 (2020). https://doi.org/10.22055/jacm.2019.30677.1766

[26] N. Rai, and S. Mondal, "Spectral methods to solve nonlinear problems: A review," Partial Differential Equations in Applied Mathematics, **4**, 100043 (2021). https://doi.org/10.1016/j.padiff.2021.100043

[27] W. Al-Kouz, C.S. Reddy, M.S. Alqarni, and B. Mahanthesh, "Spectral quasi-linearization and irreversibility analysis of magnetized cross fluid flow through a microchannel with two different heat sources and Newton boundary conditions," The European Physical Journal Plus, **136**(6), 645 (2021). https://doi.org/10.1140/epjp/s13360-021-01625-3

[28] E.E. Tzirtzilakis, and G.B. Tanoudis, "Numerical study of biomagnetic fluid flow over a stretching sheet with heat transfer," International Journal of Numerical Methods for Heat & Amp Fluid Flow, **13**(7), 830–848 (2003). https://doi.org/10.1108/09615530310502055

[29] H. Muzara, and S. Shateyi, "Magnetohydrodynamics Williamson Nanofluid Flow over an Exponentially Stretching Surface with a Chemical Reaction and Thermal Radiation," Mathematics, **11**, 2740 (2023). https://doi.org/10.3390/math11122740

[30] A. Srinu, K.S. Reddy and N. Amar, "Radiation and inclined magnetic field effects on Williamson fluid flow above a stretching sheet in the existence of velocity, thermal, and concentration slips", Partial Differential Equations in Applied Mathematics, **9**, 100611 (2024). https://doi.org/10.1016/j.padiff.2023.100611

[31] M. Faizan, M. Ajithkumar, M.V. Reddy, M.A. Jamal, B. Almutairi, N.A. Shah, and J.D. Chung, "A theoretical analysis of the ternary hybrid nano-fluid with Williamson fluid model," Ain Shams Engineering Journal, **15**, 102839 (2024). https://doi.org/10.1016/j.asej.2024.102839

[32] T. Salahuddin, and Muhammad Awais, "Thermal and solutal transport by Cattaneo-Christov model for the magnetohydrodynamic Williamson fluid with joule heating and heat source/sink," Heliyon, **10**, e29228 (2024). https://doi.org/10.1016/j.heliyon.2024.e29228

[33] Z. Liu, S. Li, T. Sadaf, S.U. Khan, F. Alzahrani, M.I. Khan, and S.M. Eldin, "Numerical bio-convective assessment for rate type nanofluid influenced by Nield thermal constraints and distinct slip features", Case Studies in Thermal Engineering, **44**, 102821 (2023). https://doi.org/10.1016/j.csite.2023.102821

БІОМАГНІТО-ГІДРОДИНАМІЧНИЙ ПОТІК РІДИНИ ВІЛЬЯМСОНА ТА ТЕПЛОПЕРЕНОС ЧЕРЕЗ ПОВЕРХНЮ, ЩО РОЗТЯГУЄТЬСЯ: СПЕКТРАЛЬНИЙ КВАЗІЛІНЕАРИЗАЦІЙНИЙ ПІДХІД

Кайраваді Суреш Бабу[b], **Вангала Сугунамма**[a], **Вамсі Крішна Нарла**[c]

[a] *Університет Шрі Венкатешвара, Тірупаті, АР, 517502, Індія*

[a] *Інженерно-технологічний інститут Гокараджу Рангараджу, TG, Індія*

[c] *GITAM вважається університетом, факультет математики, Хайдарабад, 502329, Індія*

Потік і теплопередача рідини Вільямсона, підданої магнітному полю, аналізуються та досліджуються методом спектральної квазілінеаризації (SQLM). Рівняння, пов'язані з імпульсом і енергією, отримані з рівнянь Нав'є-Стокса з урахуванням неньютонівських ефектів, в'язкої дисипації, магнітних сил і сили Лоренца. Взаємодія електропровідної рідини з магнітним полем створює силу Лоренца, яка суттєво змінює поведінку потоку, застосовуючи силу опору проти швидкості рідини. Метод ефективно лінеаризує нелінійні рівняння, забезпечуючи точні рішення за допомогою спектрального методу. Чисельні результати підкреслюють вплив параметрів рідини Вільямсона, інтенсивності магнітного поля та джерел тепла на поля швидкості та температури, пропонуючи зрозуміти поведінку рідини в промислових застосуваннях, що включають неньютонівські рідини та магнітні поля.

Ключові слова: *рідина Вільямсона; параметр джерела тепла; магнітний диполь; сила Лоренца та метод спектральної квазілінеаризації*